Adsorptive interaction of peroxymonosulfate with graphene and catalytic assessment via non-radical pathway for the removal of aqueous pharmaceuticals

Rafael R. Solís[1,*], Ismael F. Mena[2], Mallikarjuna N. Nadagouda[3], Dionysios D. Dionysiou[1]

[1]Environmental Engineering and Science program, Department Chemical and Environmental Engineering, University of Cincinnati, Cincinnati OH 45221-0012 (USA)

[2]Departmento de Ingeniería Química, Facultad de Ciencias, Universidad Autónoma de Madrid, Campus de Cantoblanco, Madrid 28049 (Spain)

[3]Department of Mechanical and Materials Engineering, Wright State University, Dayton, Ohio 45324 (USA)

*To whom correspondence should be addressed: Rafael Rodríguez Solís (rodrigr2@ucmail.uc.edu)

Abstract

Graphene has been applied as a catalyst in peroxymonosulfate (PMS) activation for the removal of pharmaceuticals in water. Firstly, a kinetic adsorption study of PMS was developed, fitting the results to the Elovich's equation. Moreover, the influence of the main variables in the adsorptive process such as pH, initial PMS concentration, and graphene dose were assessed. Secondly, the degradation of diclofenac as a target compound was studied comparing PMS-catalytic versus adsorption processes. PMS-catalytic process enhanced the removal of the micropollutant if compared to adsorption when using a low dose of graphene (less than 50 mg L^{-1}) or after surface saturation. Studies using radical scavengers suggested the lack of radicals in the process, suggesting the non-radical activation of PMS. Thirdly, the adsorption *versus* PMS-catalytic processes were also compared for the oxidation of a mixture of three antibiotics (norfloxacin, tetracycline and sulfamethoxazole) with different chemical structure. PMS-catalytic activation was more effective for the removal of those

compounds that presented less affinity towards adsorption onto the graphene surface. Finally, characterization of the fresh and PMS-treated material was performed. Graphene demonstrated to be stable after its use as catalysts in PMS activation, suffering only slight transformation of the surface oxidation groups.

Keywords: graphene, peroxymonosulfate activation, adsorption, diclofenac, antibiotics, water treatment, pharmaceuticals

1. INTRODUCTION

Since graphene monolayer was first reported in 2004 [1], diverse applications based on graphene-derived materials have been launched. Graphene is defined as a single sheet of sp^2 hybridized carbon, defining a 2D carbonaceous crystalline allotrope with regular hexagonal pattern. This bonding carbon lattice allows graphene to present excellent characteristics such as high thermal conductivity, high mechanical strength, electrical conductivity, high electronic capacity and excellent optical properties, among others [2]. Graphene's properties enable it to be a promising material for many applications in the field of water treatment, such as its flexibility and hydrophobicity to build membranes of small pores for applications in filtration [3,4] and desalination [5,6]. Moreover, due to the mentioned properties, graphene is under research as nano-adsorbent [7–9] and nano-catalyst [10–12].

Water treatment processes should address the new challenges and needs that current Society demands. For example, most wastewater treatment plants cannot completely remove trace organic chemicals, including Contaminants of Emerging Concern (CECs) [13]. The current implemented wastewater treatment processes, usually, biological-based on activated sludge, do not degrade or only slightly oxidize these contaminants, in some cases to other recalcitrant intermediates, and thus a significant portion of these trace organic CECs are present in the effluent. Although the concentration of CECs in

52 the wastewater effluents is typically very low, they are frequently referred as
53 micropollutants since are typically reported at μg L^{-1} or ng L^{-1} level, the consequences
54 of their exposure in the environment in the long term are still largely unknown and
55 further research to get more insights is underway [14,15]. From all the feasible
56 treatment solutions proposed by the research community, Advanced Oxidation
57 Processes (AOPs) based on either hydroxyl radicals [16] or sulfate radicals [17] are a
58 promising option because of their effectiveness in the oxidation of a wide range of
59 recalcitrant organic substances [18,19]. However, the main concern of the use of S
60 containing oxidants is the release of sulfate anions after the treatment. This aspect could
61 be considered acceptable depending on the oxidant dose added and the further
62 application of the treated effluent.

63 Sulfate radical-based AOPs are processes that rely on the production of sulfate
64 radical as the main oxidation species by the breakage of the peroxy bond of
65 peroxymonosulfate (PMS) or peroxydisulfate (PDS). The generation of sulfate radicals
66 may be triggered by thermal [20], radiation [21], or catalytic activation [22,23], among
67 other methods. Much research has been conducted regarding the catalytic activation of
68 these species with metal-based substances, either as dissolved metals or as metals
69 immobilized on supports. However, the main concerns regarding the use of metallic
70 catalysts are related to toxicity concerns, if they are released to the treated effluent, and
71 the high cost for applications with metal catalysts. In this sense, graphene has emerged
72 as a promising material applicable to catalytic AOPs [20]. The activation of PMS or
73 PDS through the use of carbonaceous catalysts (i.e. activated carbon, graphite, carbon
74 nanotubes, nanodiamonds or graphene) [24–29] is attracting significant research interest
75 since activated carbon is already established and economically feasible in many water
76 treatment plants. The addition of oxidants enables the removal of adsorbed species as

77 the carbon material is used as a catalyst and not as an adsorbent that needs frequent
78 regeneration. The carbocatalysis of PMS and PDS is still under research, and a non-
79 radical pathway is thought to take place via the formation of $^1O_2$ species [24,30,31]. It is
80 well known that the self-decomposition of PMS at alkaline conditions (pH>pK_a) slowly
81 generates singlet oxygen [32]

82 $$HSO_5^- + SO_5^{2-} \xrightarrow{k=0.2 M^{-1}s^{-1}} HSO_4^- + SO_4^{2-} + {}^1O_2 \quad (1)$$

83 Similarly, singlet oxygen release has been described during the autodecomposition of
84 PDS [33]. Recently, it was reported that the reaction of PMS and benzoquinone
85 involves the generation of $^1O_2$ through the formation of a dioxirane intermediate [32].
86 Diverse studies have shown uncertainties and different conclusions about the formation
87 of radical, non-radical pathway, or combination of both. However, it has been suggested
88 that the non-radical pathway is the main contribution in carbocatalysis. The low
89 proportion of oxygenated groups and carbon edges (sp^2-conjugation with unpaired
90 electrons) are usually the active sites to interact with the peroxide bond of PMS [30].

91 Few works have focused on the interaction of peroxymonosulfate and graphene [34],
92 and those available do not report the kinetic study of PMS evolution during these
93 processes. The chemisorption of PMS onto reduced graphene oxide has been recently
94 studied from a thermodynamic point of view [26]. The research available related to
95 PMS and graphene is focused on the evaluation of degradation of target compounds
96 such as phenol [24,35–37], dyes [36] or Bisphenol A [38].

97 This work presents the study of PMS interaction onto commercial graphene, focusing
98 the interest on the kinetics of PMS adsorption, and how the main variables (pH, PMS
99 dose and graphene dose) affect the process. The characterization of the material before
100 and after the treatment was also performed. Diclofenac was chosen as the target CEC,

and the efficiency of adsorption *versus* catalysis on the pollutant's removal processes was studied. The role of the main process parameters (pH, graphene dose, diclofenac and PMS initial concentrations, reusability of the solid, etc.) was investigated with respect to the kinetics of the process. Scavenging probe studies revealed the importance of the non-radical pathway. PMS was found to be the most efficient oxidant compared to other oxidants such as hydrogen peroxide (H_2O_2), persulfate, and peracetic acid. Finally, the process was evaluated for the degradation of different types of antibiotics.

2. EXPERIMENTAL

2.1. Chemicals

Diclofenac sodium salt (DCF, $C_{14}H_{10}Cl_2NNaO_2$, CAS: 15307-79-6, Sigma-Aldrich®), norfloxacin ($C_{16}H_{18}FN_3O_3$, CAS:70458-96-7, Alfa Aesar), tetracycline ($C_{22}H_{24}N_2O_8$, CAS: 60-54-8, Alfa Aesar) and sulfamethoxazole ($C_{10}H_{11}N_3O_3S$, CAS: 723-46-6, TCI America) were of analytical grade and used as received. Oxone® ($2KHSO_5 \cdot KHSO_4 \cdot K_2SO_4$, CAS: 37222-66-5) from Sigma-Aldrich® was used as a source of peroxymonosulfate (PMS). Hydrogen peroxide and potassium peroxydisulfate (PDS) were acquired from Fisher®. Peracetic acid (PAA) was obtained from Sigma-Aldrich®. Commercial graphene nanoplatelets aggregates (CAS: 7782-42-5, 500 $m^2 g^{-1}$, Alfa Aesar®) were used as received. All the chemicals used for analytical purposes were of analytical grade and purchased from Sigma-Aldrich®. Test and analytical solutions were prepared with ultrapure water from a Barnstead™ E-Pure™ device (resistivity >17.5 MΩ·cm). HPLC-grade acetonitrile from Fisher Chemicals® was used for HPLC analysis.

2.2. Experimental procedure

All tests were carried out in glass cylindrical beakers in which 250 mL of aqueous solution was added. The desired amount of PMS, from a concentrated solution (generally 0.01 or 0.1 M), and graphene were added under magnetic stirring. For PMS adsorption study, initial PMS concentration was within 0.39-1.17 mM and graphene 0.30-1.24 g L^{-1}. Diclofenac (DCF) removal was evaluated under the following conditions: graphene dose, 10-250 mg L^{-1}; initial PMS concentration, 0.1-1.0 mM; initial DCF concentration, 1-10 mg L^{-1}; pH (buffered with H_3PO_4 mM when necessary), 3-9.

At different times, samples were extracted and filtered with 0.22 μm PVDF filters. Samples for HPLC analyses were quenched with sodium thiosulfate. Catalyst recovery, when required, was completed by filtration of the solution (0.45 μm filters) and drying overnight at 100ºC. In these reusing experiments, solution volume was proportionally decreased to balance the catalyst loss after each cycle and keep constant the graphene dose.

2.3. Aqueous analyses

The concentration of aqueous organic pollutants was determined by High-Pressure Liquid Chromatography coupled to Diode Array Detection (HPLC-DAD). The instrument used was an Agilent® 1100. The chromatographic separation took place in a Supelco discovery® HS C18 column (15 cm x 4.6 mm, 5μm), thermally kept at 25 ºC. For individual analysis of diclofenac, a mixture of 70% of acetonitrile and 30% of acidified water (0.1% v/v of formic acid) was pumped at a rate of 0.3 mL min^{-1} followed by quantification at 221 nm. The mixture of three antibiotics (norfloxacin, tetracycline, and sulfamethoxazole) was analyzed by pumping 1 mL min^{-1} of 15:85

147 acetonitrile: acidified water (0.1% v/v formic acid), the quantification registered at 260
148 nm (except for norfloxacin, 286 nm). Limit of detection (LOD) and quantification
149 (LOQ) were obtained from calibration curves [39] (see Table S1). The concentration of
150 peroxymonosulfate (PMS) was colorimetrically determined by DPD (N,N-Dimethyl-
151 1,4-phenylenediamine) oxidation at buffered media [40].

152 **2.4. Solid characterization**

153 Surface area and porous properties were analyzed by nitrogen adsorption-desorption
154 isotherm in a Micromeritics® Tristar 3000 apparatus (-196 ºC, specific surface area
155 resolution 0.01 m^2 g^{-1}). The degasification of the samples (~120 g) was performed
156 during 24 h at 120 ºC using N_2 as purging gas.

157 The Scanning Electron Microscopy used was a Thermo Scientific™ Apreo™ device
158 equipped with an EDAX elemental analysis detector. The accelerating voltage was
159 within 1-30 kV at the maximum amplification.

160 Transmission Electron Microscopy analysis was carried out in an FEI-Philips CM-20
161 TEM device equipped with LaB_6 filament, EDX analysis, and Orius CCD camera. The
162 maximum accelerating voltage was 200 kV, the image resolution was 0.27 nm, and
163 maximum magnification was 750,000X. For analysis, graphene powder was dispersed
164 in pure isopropyl alcohol under vortex agitation. After that, a drop of the supernatant
165 was fixed on a copper grid and dried at room temperature until picturing.

166 X-Ray Diffraction (XRD) was performed in a Panalytical (Expert) 2-theta
167 diffractometer working with monochromatic CuKα radiation (wavelength, 1.54 Å) and
168 angle range (2θ) within 2 and 90º.

169 Fourier Transform InfraRed (FTIR) spectroscopy was carried out in an Agilent®
170 Cary 600 series FTIR spectrometer, at wavenumber ranging from 650 to 4000 cm^{-1}.

171 Surface oxidation states of oxygen were investigated by employing PHI VersaProbe
172 III X-ray Photoelectron Spectroscopy (XPS) microprobe instrument with Kα Al
173 monochromatic radiation (1486.68 eV).

174 The pH of point zero charge (pH_{pzc}) of graphene in aqueous solution was obtained by
175 standard acidic-base titration [41]. Briefly, 120 mg of the solid was added to 40 mL of
176 the water solution and kept under stirring. The initial desired pH (within 2 and 12) was
177 adjusted by adding 0.1 M HNO_3 and NaOH solutions. The pH drift-test was concluded
178 until the final pH was recorded as stable. The pH value at which the experimental curve
179 undergoes $pH_{initial}$=pH_{final} was estimated as the pH_{pzc}.

180 **3. RESULTS AND DISCUSSION**

181 **3.1. Kinetics modeling of PMS adsorption onto graphene. Influence of variables**

182 Adsorption of peroxymonosulfate onto carbonaceous materials is thought to take
183 place via chemisorption [26]. The presence of electrostatic interactions between PMS
184 and π-π bonds of graphene plays an important role [42]. To study the kinetic of PMS
185 adsorption onto graphene, a Design of Experiment (DOE) using Surface Response
186 Methodology (RSM) was carried out selecting initial PMS concentration, graphene
187 dose, and pH as the essential variables to study. Design Expert® software was used to
188 build the Central Composite Design (CCD) with a bunch of 20 experiments (6
189 repetitions of the central point). Fig. 1A depicts the conditions of the set of tests
190 launched, the range for each variable being the following: $C_{PMS,0}$ from $5 \cdot 10^{-4}$ to 10^{-3} M;
191 $C_{graphene}$ from 0.3 to 1.0 g L^{-1}; and pH from 5 to 9. The PMS concentration decay in the
192 presence of graphene was monitored and results showed a fast decrease which slowed
193 down after the first minutes. Fig. 1B shows, as an example, the kinetic of PMS
194 concentration evolution for the central point of the selected CCD.

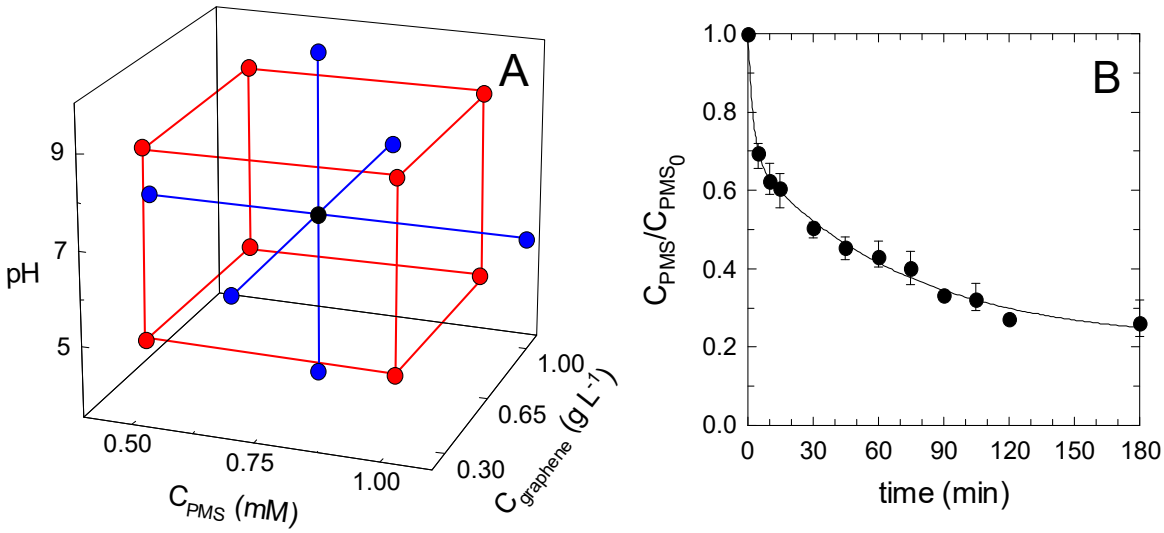

Figure 1. CCD applied to peroxymonosulfate adsorption onto graphene. Figure 1A, the experimental conditions of the selected Central Composite Design (black, center point; red, embedded factorial points; blue, star points). Figure 1B, the evolution of aqueous PMS-concentration *versus* time for the central point, experimental conditions: $C_{PMS,0}$=7.5 mM; $C_{graphene}$=0.65 g L^{-1}; pH=7; continuous line, kinetics fitting

At first sight of the profiles observed for the PMS evolution, since a stable plateau seems to be reached, no predominance of catalytic decomposition should be assumed. The main mechanism for PMS disappearance takes place by adsorption. Therefore, the experimental data were fitted to adsorption kinetic models. From all the empirical models available in the literature to describe the process of adsorption, the Elovich's model was selected, as it better fitted than pseudo-first or pseudo-second order models. This model was first applied to fitting gas chemisorption processes [43]. Nonetheless, it has also been widely used to describe the adsorption processes of aqueous organic pollutants [44]. According to Elovich's equation, the kinetics of PMS adsorption can be described as follows:

$$\frac{dq_{PMS}}{dt} = ae^{-\alpha q} \qquad (2)$$

where q_{PMS} is the PMS adsorption capacity; a represents the initial adsorption rate, and α is the adsorption rate. To simplify Elovich equation, Chien-Clayton assumed that (aα)>>1 [45]. Taking the boundary conditions as $q_t=0$ for t=0 and $q_t=q_t$ at t=t, eq. (2) can be transformed into the following:

$$q_{PMS} = \alpha \ln\left(a\frac{1}{\alpha}\right) + \alpha \ln(t) \quad (3)$$

As the PMS adsorption capacity is defined as:

$$q_{PMS} = \frac{C_{PMS_0} - C_{PMS}}{C_{graphene}} \quad (4)$$

eq. (3) can be expressed as:

$$C_{PMS} = C_{PMS_0} - k\left[\ln\left(a\frac{1}{\alpha}\right) + \ln(t)\right] \quad (5)$$

where $k=\alpha \cdot C_{graphene}$. A representation of C_{PMS} *versus* ln(t) gives a straight line, from the slope of which it is possible to obtain k. Eq. (5) was used to model the experimental data. A good correlation was found, with $R^2>0.97$ in most cases. Fig. 1B depicts the evolution of normalized PMS concentration and the goodness of the proposed fitting for the results of the central point.

The constant k was selected as the response for the Surface Response Methodology in the CCD, assessing the influence of the three variables chosen in the process. The results attained for each experimental series is accomplished in Table S2. From the analysis of Expert-Design® software, the best output with a reasonable agreement between experimental k and model was a linear plus interaction regression:

$$k^{-1} = \left(\alpha C_{graphene}\right)^{-1} = b_0 + b_1 C_{PMS} + b_2 C_{graphene} + b_3 pH + b_4 C_{PMS} C_{graphene} + \\ + b_5 C_{PMS} pH + b_6 C_{graphene} pH + b_7 C_{PMS}^2 + b_8 C_{graphene}^2 + b_9 pH^2 \quad (6)$$

Table 1 summarizes the statistical characteristics of the adjustment, with a reasonable regression coefficient (adjusted R^2=0.9416). Coded values for b_i constant can serve to know the relative importance of each variable and their interactions. Hence, a decreasing impact following the order PMS initial concentration > graphene dose > pH was observed. From the ANOVA analysis, the p-values obtained reveal higher significance ($p<0.05$) of the first-order terms if compared to the second-order interactions. More detailed statistical description can be found in the supplementary material (Table S2 and Fig. S1).

Table 1. Modeling of PMS adsorption onto graphene. Statistical results of the Central Composite Design after analysis with Design-Expert®

Factor	Coded value	p-value	ANOVA	Value
b_0	8261.12	-	**R^2**	0.9693
b_1	-3146.79	< 0.0001	**Adjusted R^2**	0.9416
b_2	-1968.35	< 0.0001	**Predicted R^2**	0.8559
b_3	-1652.74	< 0.0001	**Adequate precision***	22.0211
b_4	573.66	0.0918	**F-value****	35.06
b_5	446.31	0.1775	**p-value (model)**	< 0.0001
b_6	598.56	0.0804	**Lack of fit**	Not significant
b_7	488.37	0.0590	**Sum squares (regression)**	$2.390 \cdot 10^8$
b_8	387.03	0.1222	**Sum squares (residuals)**	$7.574 \cdot 10^6$
b_9	378.27	0.1299	**Lack of fit**	Not significant

*Adequate precision measures the signal to noise ratio. A ratio greater than 4 is desirable.
**The Model F-value of 35.06 implies the model is significant.

The relative impact of the variables can be identified not only from the coded values (see Table 1) but also visually from the surface 3D responses depicted with the model. Fig. 2 shows the 3D graphs for the k constant, at three selected pH values. As inferred from the figure, the influence of PMS concentration is higher than those observed for graphene dose. All the variables exerted a positive effect on the range studied. The higher the values of pH, C_{PMS} or $C_{graphene}$ were in the ranges studied, the better the

250 performance of PMS adsorption reached was. Interesting is the better performance as
251 pH increases. At pH>pH_{pzc}, the surface of the solid is expected to be negatively charged
252 as well as HSO_5^- molecule. Therefore, other mechanism different from electrostatic
253 repulsions must apply.

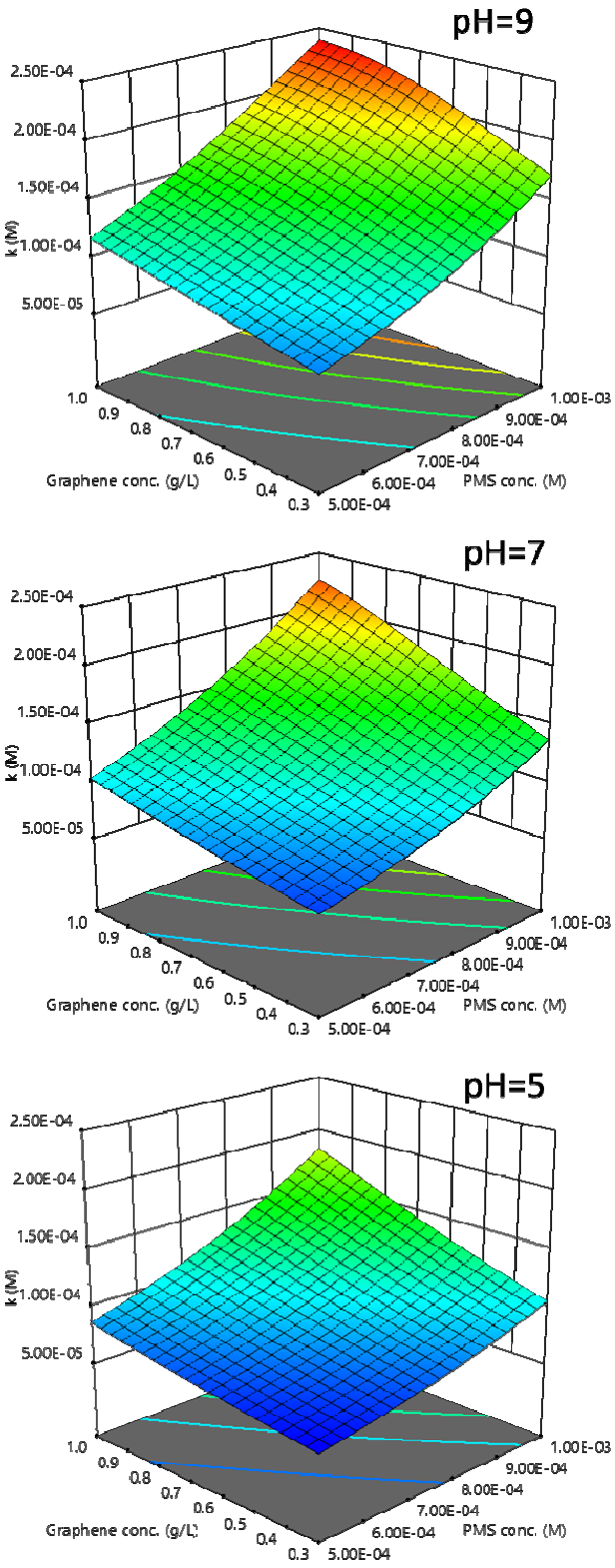

254

255 **Figure 2.** RSM applied to the kinetics of peroxymonosulfate adsorption onto graphene.

256 3D surfaces for the predicted k-values at three different pH values (9, 7, 3).

257 **3.2. Diclofenac removal by peroxymonosulfate-graphene system**

258 *3.2.1. Adsorption versus PMS catalysis. Kinetics*

259 The behavior of the combination of peroxymonosulfate and graphene as oxidative
260 technology was assessed for the removal of diclofenac as a target aqueous pollutant.
261 Hence, a series of experiments were conducted to evaluate the catalytic potential of
262 graphene combined with PMS. Adsorption of DCF on diverse carbon materials has been
263 studied in previous works. Diverse performances have been reported depending on the
264 kind of material, surface area, particle size, presence of surface oxygenated groups, and
265 other factors. Generally, the kinetics fit a pseudo-second order model and the isotherm
266 can be explained by Langmuir equation. Table 2 summarizes the maximum capacity of
267 adsorption, specific surface area, models used for kinetics and isotherms for some recent
268 works on carbon-based adsorbents available in literature.

Table 2. Summary of studies with carbonaceous materials applied for DCF adsorption.

Material	Specific surface area (m^2 g^{-1})	Kinetic model	Equilibrium model		Ref.
			Model	Maximum adsorption capacity (mg g^{-1})	
Oxidized AC[1]	704	Pseudo-second order	Langmuir	487	[46]
Commercial AC	1016	Pseudo-second order	Langmuir	83	[46]
GAC[2]	997	-	Freundlich	297	[47]
GAC	1156	Pseudo-second order	Langmuir	385	[48]
AC from olive Stone	83.7	Pseudo-second order	Langmuir	11.0	[49]
AC from agricultural byproducts	793	Pseudo-second order	Langmuir	56.2	[50]
AC from cocoa shell	619	Pseudo-second order	Liu	63.4	[51]
Carbon nanofibers	199	-	Langmuir	29.9	[52]
Multi-walled carbon nanotubes	162	-	Langmuir	41.4	[52]
Multi-walled carbon nanotubes	382	Pseudo-second order	Freundlich	209	[53]
Multi-walled carbon nanotubes	13	Pseudo-second order Intraparticle diffusion	Langmuir	7.26	[54]
GO[3]	-	-	Langmuir	500	[55]
rGO[4]	98	Pseudo-second order	Liu	59.6	[56]
rGO aeorgel	132	Pseudo-first order	Langmuir	342	[57]

[1]AC: Activated Carbon; [2]GAC, Granular Activated Carbon; [3]GO, Graphene Oxide; [4]rGO, reduced Graphene Oxide.

Fig. 3A depicts the normalized DCF concentration evolution *versus* time, undergone for adsorption and PMS-aided catalysis. At first sight, graphene presented a high adsorption capacity of DCF, the kinetics is slightly improved in the presence of PMS when graphene dose was higher than 100 mg L^{-1}. The initial rate of DCF disappearance was estimated to be 0.582 mg DCF min^{-1} for adsorption *versus* 0.850 mg DCF min^{-1} for PMS reaction when working with 100 mg L^{-1} of graphene, which means that the catalytic process accelerated the process initially *circa* 1.461 times. At graphene doses of 20 mg L^{-1} the initial rate constant was 1.535 times higher when PMS was added if compared to adsorption. Moreover, the presence of PMS improved the elimination of DCF especially at a low dose of graphene, achieving 84% after 2 hours of treatment if compared to 64% of the adsorption process.

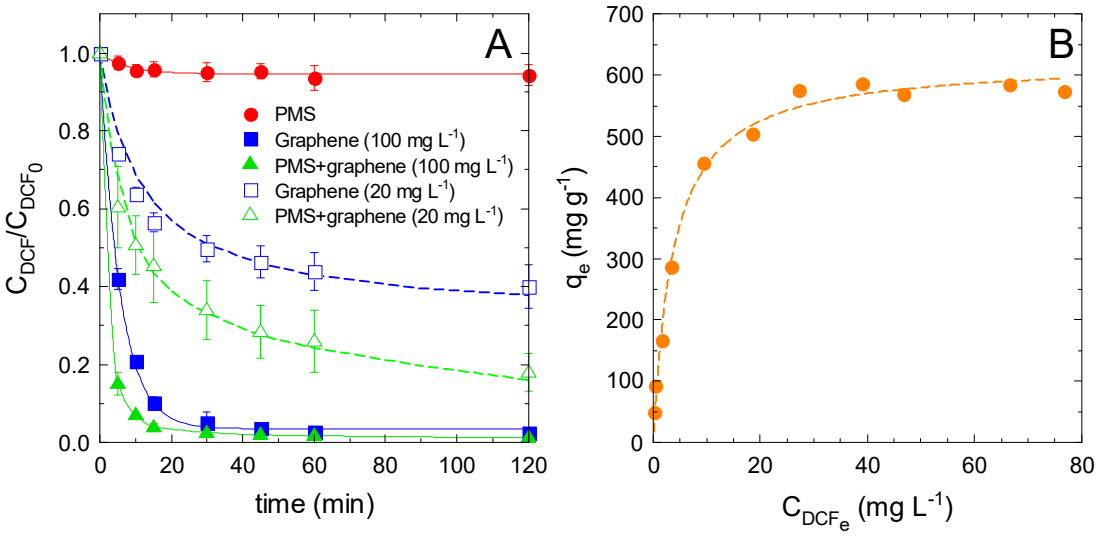

Figure 3. (A) Adsorption *versus* PMS-catalysis of DCF onto graphene. Experimental conditions: V=250 mL; $C_{DCF,0}$=5 mg L^{-1}; $C_{PMS,0}$=0.1 mM; $C_{graphene}$=100 or 20 mg L^{-1}; $pH_{initial}$=4.0-4.4 (unbuffered). (B) Adsorption isotherm of DCF onto graphene. Experimental conditions: V=50 mL; $C_{graphene}$=100 mg L^{-1}; $C_{DCF,initial}$=100 to 10 mg L^{-1}; $pH_{equilibria}$=3.6-4.0. Dashed lines: modeled kinetics (A) and isotherm (B)

From all the pseudo empirical approaches available to the adsorption kinetics followed during the DCF removal, the pseudo-second-order adsorption model seems to

290 best describe the results, as is also used in most of adsorption graphene-based materials
291 [7]. This adsorption model identifies the adsorption process as second-order chemical
292 reaction as follows:

293 $$\frac{dq_{DCF}}{dt} = k_2(q_{DCF_e} - q_{DCF})^2 \quad (7)$$

294 where q_{DCF} is the DCF adsorption capacity, $q_{DCF,e}$ is the DCF adsorption capacity at
295 equilibrium, and k_2 is the adsorption constant of the model. Eq. (7) can be transformed
296 into DCF concentration, leading to:

297 $$-\frac{dC_{DCF}}{dt} = \frac{k_2}{C_{graphene}}(C_{DCF} - C_{DCF_e})^2 \quad (8)$$

298 Differential Eq. (8) was numerically solved, i.e. Euler's method, and adjusted to the
299 experimental data by non-linear regression.
300 To kinetically explain the decay of DCF in PMS-catalysis with graphene, a reaction
301 term was tentatively added to Eq. (8):

302 $$-\frac{dC_{DCF}}{dt} = \frac{k_2}{C_{graphene}}(C_{DCF} - C_{DCF_e})^2 + k_{obs}C_{DCF} \quad (9)$$

303 where the rate constant k_{Obs} is a pseudo-first-order rate constant of the catalytic reaction
304 launched by PMS.
305 Eqs. (8) and (9) were successfully fitted to the experimental data in those cases in which
306 the surface of graphene was completely saturated with DCF. The dashed lines presented
307 in Fig. 3A depicts the modeling results of DCF decay, either in presence or absence of
308 PMS, and the values attained for that simulating kinetics are available in Table 3. In the
309 next section, in which the influence of the operational variables is presented, Eqs. (8)
310 and (9) were also used as a tool to explain the observed kinetics.

311 **Table 3.** Adsorption *versus* PMS-catalysis of DCF onto graphene at low concentration
312 (20 mg L^{-1}). Adjusted parameters to the pseudo-second-order model kinetics

Pseudo-second order parameters	System	
	Graphene	Graphene+PMS
k_2, g graphene (mg DCF)$^{-1}$ min^{-1}	1.229	1.389
$C_{DCF,e,}$ mg L^{-1}	1.588	1.070
$k_{Obs}\cdot 10^3$ (min^{-1})	-	5.92
R^2	0.999	0.999

The adsorption capacity of graphene-based materials is highly related to the structure of the molecule, and therefore, the interactions that may be taking place onto the surface of the material. These can mainly be summarized as electrostatic, hydrogen bonds if the surface is partially oxygenated, and π-π interactions between adsorbate and adsorbent [44]. The adsorption isotherm of DCF onto the commercial graphene was obtained and the experimental data were successfully fitted to the Langmuir model [7,58], which assumes equal possibility to the physical and chemical binding and homogeneous surface:

$$q_{DCF,e} = \frac{q_{DCF,max} k_L C_{DCF,e}}{1 + k_L C_{DCF,e}} \quad (10)$$

where $q_{DCF,e}$ is the adsorption capacity of DCF at equilibrium; $q_{DCF,max}$ is the maximum monolayer capacity of DCF; $C_{DCF,e}$ is the DCF concentration reached equilibrium; and k_L is the constant of the Langmuir model. Eq. (10) was solved by non-linear regression fitting, providing a satisfactory description (R^2=0.98; see Fig. 3B) with the following values for the constants: $q_{DCF,max}$=610.8 mg DCF (g graphene)$^{-1}$; and k_L=0.279 L (mg DCF)$^{-1}$. The maximum capacity value obtained is in good agreement with the reported previously for graphene oxide (500 mg DCF per g of graphene) [59].

The direct reaction between organic substances and PMS has been reported to be thermodynamically feasible for pollutants of emerging concern [60–63]. PMS is also a well-known soft oxidant agent used in organic synthesis of diverse substances such hydrocarbons, hydroxylated compounds, carbonyl organics, amines, nitrogen heterocycles, and organic containing sulfur, phosphorous and halogen atoms [64].

However, no direct reaction between DCF and PMS was achieved under the conditions tested in Fig. 3A at a molar ratio of DCF: PMS~1:6. Nevertheless, moderate conversion of DCF after 2 hours of direct reaction with PMS was observed at higher molar ratios (39.1%, 60.2%, and 66.8% at DCF: PMS molar ratio of ~1:30, ~1:60, and ~1:600, respectively; results not shown).

3.2.2. PMS catalysis with graphene. Influence of process variables

The influence of the main process variables affecting the degradation of DCF by PMS+graphene catalytic system was assessed. Graphene dose, pH, PMS, and DCF initial concentration were selected as the most relevant. Fig. 4 depicts the results obtained.

As shown in Fig. 4A, graphene dose was found to be one of the most important variables since the catalytic effect on DCF removal was quite influenced by the great adsorption capacity of graphene. A stable plateau of C_{DCF} was observed during the adsorption process when graphene dose was within 10 and 50 mg L^{-1}, due to the saturation of the surface. The addition of PMS under these conditions improved the initial DCF degradation with a slower linear stage. Notably, 50 mg L^{-1} of graphene was capable of completely removing DCF from the aqueous media in 60 min. The higher dose of graphene led to complete adsorption of DCF, and the addition of PMS slightly accelerated the process.

pH exerts an important role since pK_a of DCF and PMS, in conjunction with the pH of the point of zero charge (pH_{pzc}) of graphene, determine the electrical interactions between the adsorbate and solid surface. pH_{pzc} for fresh graphene was found to be 5.37 (see Fig. S2). Aqueous $pH<pH_{pzc}$ means surface positively charged; therefore, high attraction potential for anions. DCF's pK_a is 4.15 while the second dissociation constant

358 for PMS into SO_5^{2-} has a pK_a=9.4 [65]. Adsorption of both species is expected to play
359 the main role at pH lower than pH_{pzc}. At pH below pH_{pzc}, higher adsorption affinity of
360 DCF (neutral) is expected if compared to pH>pH_{pzc}. At basic pH, it is expected that the
361 electrostatic repulsion between graphene surface and deprotonated DCF impedes the
362 adsorption process. As can be observed from Fig. 4B, there is a negative influence of
363 increasing pH from 3 to 9, during PMS catalytic process. A less positively, or
364 negatively, charged graphene surface would disfavor adsorption of DCF. The
365 enhancement of catalysis with respect to adsorption process is higher at acidic
366 conditions. The raise of pH during adsorption of PMS, contrary to what expected
367 according to the same reasoning carried out for DCF, exerted a positive effect. That
368 indicates that another mechanism different from electrostatic repulsion might play an
369 important role for PMS.

370 The influence of the initial concentration of PMS is frequently evaluated in catalytic
371 systems in order to assess the optimum dose. Some experiment at different initial PMS
372 concentration (0.1-1.0 mM) where conducted. Although the pH was lower as the initial
373 PMS concentration was increased (unbuffered tests), the effect of pH is expected to be
374 minimal as the initial pH differs in only one unit. PMS dose exerts a positive influence
375 until reaching an optimum; after that, it starts to become negative. The higher the
376 amount of oxidant, the better the performance registered in the targeted pollutant.
377 However, as it is also observed in this system, after a certain dosage of PMS, a slightly
378 negative effect is observed. In this particular case, $C_{PMS,0}$>0.75 mM caused a partial
379 inhibition (see Fig. 4C). It is well known that when PMS is in excess, it is auto
380 consumed by radicals, triggering a scavenging effect in which the target pollutant and
381 PMS compete for the generated oxidizing species [66]:

382 $$HSO_5^- + HO^\bullet/SO_4^{\bullet-} \rightarrow SO_5^{\bullet-} + SO_4^{2-} + H^+/HO^- \quad (10)$$

383 Nevertheless, carbocatalysis with inorganic peroxides like PMS is thought to take place
384 by a non-radical pathway through singlet oxygen generation ($^1O_2$). Similarly, PMS in
385 excess seems to compete with the organic (DCF) for non-radical oxidant species. An
386 overdose of oxidant affects negatively after reaching an optimum value.

387 An increase in the initial DCF is expected to impact positively the elimination rate of
388 the organic, as proposed in Eq. 9. Since the effect of initial DCF concentration is hard to
389 be analyzed from the temporal evolution of normalized concentration, the initial rate
390 was estimated as a better tool to study this variable. Thus, as observed in Fig. 4 D1, an
391 increase of initial DCF concentration enhanced the degradation rate of the
392 micropollutant.

393

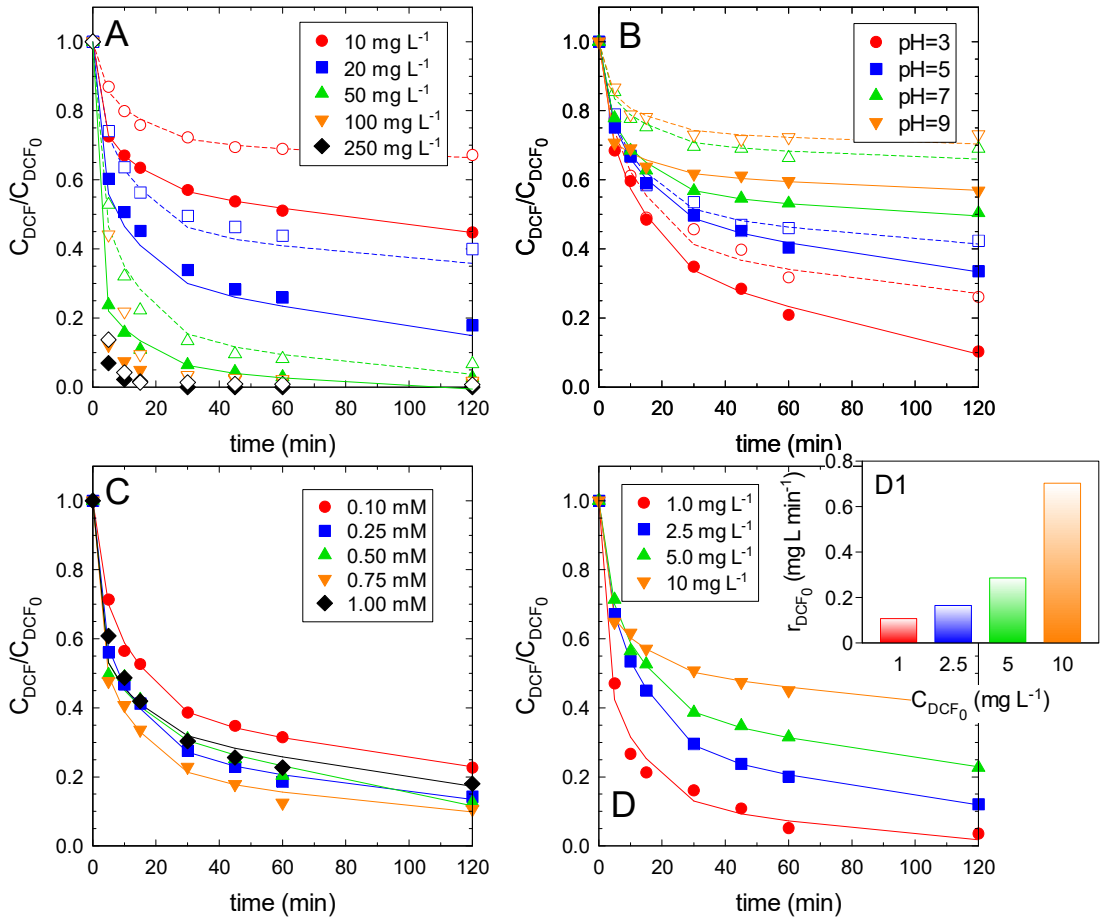

Figure 4. Operational variables influence in the removal of DCF by PMS-catalysis. (A) Influence of graphene dose (symbols filled, PMS-catalysis; empty, adsorption), experimental conditions: $C_{DCF,0}$=5 mg L^{-1}; $C_{PMS,0}$=0.1 mM (if necessary); pH=free. (B) Influence of pH, experimental conditions: $C_{DCF,0}$= 1mg L^{-1}; $C_{PMS,0}$=0.1 mM; $C_{graphene}$=20 mg L^{-1}; pH buffered (C_{H3PO4}=5 mM). (C) Influence of initial PMS concentration, experimental conditions: $C_{DCF,0}$=1 mg L^{-1}; $C_{graphene}$=20 mg L^{-1}, $pH_{initial}$=3.4-4.4 (unbuffered). (D) Influence of initial DCF concentration, experimental conditions: $C_{graphene}$= 20 mg L^{-1}; $C_{PMS,0}$=0.1 mM; pH=unbuffered.

3.2.3. Reusability of graphene in adsorption vs. reaction with PMS

The loss of activity during the catalytic process was evaluated by reusing the catalyst after 2 hours of reaction. For that purpose, the solid was recovered by filtration and dried overnight. To balance the graphene dose, the volume of the reaction was readjusted according to the catalyst loss. Fig. 5 depicts the results of the evolution of the DCF normalized concentration *versus* time during four consecutive runs in the presence

of 100 mg L^{-1} of graphene. Adsorption results during recycling are also accomplished to compare both processes.

As inferred in Fig. 5 the catalytic deactivation of graphene in the presence of PMS was minimal, and only after 3rd and 4th run ~5% of residual DCF is observed. That effect may be related to the adsorption of intermediates or final oxidation products with a better affinity towards graphene surface. Adsorption process became inefficient after the 3rd run as the active centers started to be blocked by adsorbed DCF molecules. No desorption of DCF was observed in the absence of PMS under the experimental condition tested. The use of PMS-catalysis with graphene proved to be more efficient than the adsorption process.

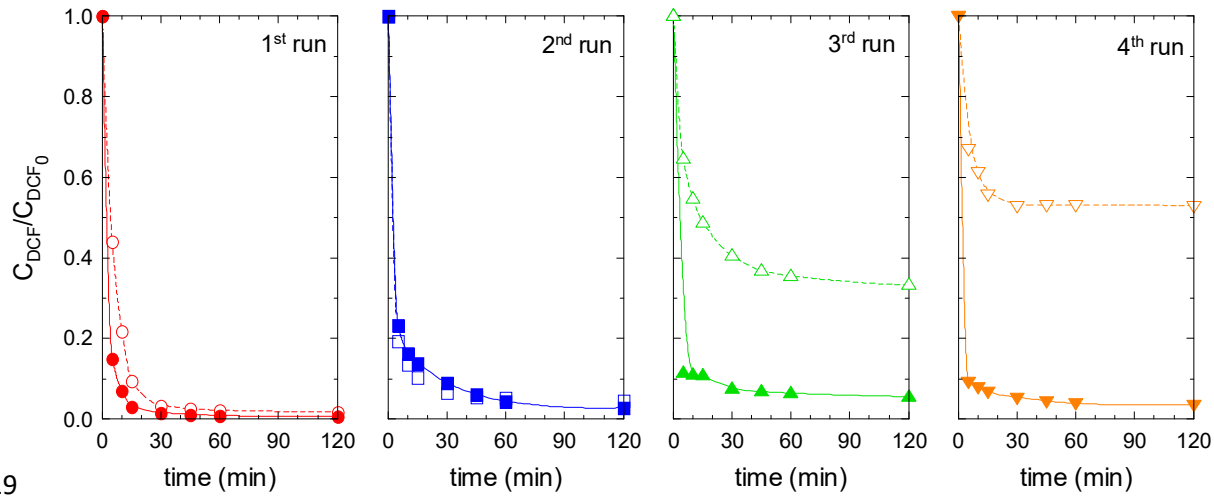

Figure 5. Graphene reusability test during adsorption (empty symbols) and PMS-catalytic (filled symbols) tests. Experimental conditions: V=250 mL; $C_{DCF,0}$=5 mg L^{-1}; $C_{PMS,0}$=0.1 mM; $C_{graphene}$=100 mg L^{-1}; $pH_{initial}$=4.0-4.4 (unbuffered).

3.2.4. Study on oxidative pathways with quenchers and PMS effectiveness compared to other oxidants

The oxidative pathway of the process that combines PMS and graphene was studied by adding scavengers that presumably suppress certain radicals or non-radical oxidative pathways. Although this technique might be controversial due to the lack of selectivity

of the available quenchers towards a specific radical; it is still useful since it allows to discern the preferential pathway. In PMS aqueous chemistry, the following main Reactive Oxidative Species (ROS) are expected to participate: $HO^{\bullet}$, $SO_4^{\bullet-}$, $O_2^{\bullet-}$ and $^1O_2$. Accordingly, different inhibitors of these oxidative pathways were tested. Results are depicted in Fig. 6.

Linear alcohols (i.e. methanol, ethanol or *iso*-propanol) react moderately fast with both hydroxyl and sulfate radicals [42]. For example, the reported values for the second-order rate constant of ethanol with hydroxyl and sulfate radicals are, respectively, in the order of 10^9 and 10^7 M^{-1} s^{-1} [21]. However, not all alcohols present similar reactivity towards superoxide anion. Methanol reacts fast with superoxide (order of 10^7 M^{-1} s^{-1}) whereas ethanol and *i*-isopropanol are more selective (10^2 M^{-1} s^{-1} and <0.1 M^{-1} s^{-1}, respectively) [67]. To distinguish the predominance of hydroxyl or sulfate radicals, *tert*-butyl alcohol (TBA) is usually used, as it reacts slower with $SO_4^{\bullet-}$ (in the order of 10^5 M^{-1} s^{-1}) than $HO^{\bullet}$ (in the magnitude of 10^8 M^{-1} s^{-1}) [42]. The testing assays in the presence of ethanol or *tert*-butyl alcohol did not inhibit the DCF decay during the process, which may be indicative of no predominance of $HO^{\bullet}/SO_4^{\bullet-}$ species in the process.

p-benzoquinone (pBZQ) is frequently used as superoxide radical quencher in PMS oxidation technologies [42]. Even so, pBZQ is also very reactive with $HO^{\bullet}$ (rate constant, in the range of 10^9 M^{-1} s^{-1} [68]) and $SO_4^{\bullet-}$ (in the magnitude of 10^8 M^{-1} s^{-1} [69]). The direct reaction of pBZQ and PMS, under alkaline pH, has been recently reported as an effective technology to produce $^1O_2$ due to the catalytic effect of HO^- anions [32]. Since the pH of the reaction during the experiment was below 5, this latter reaction can be disregarded. From the results with EtOH and TBA, it can be accepted that if pBZQ affects the kinetics is due to the influence of superoxide radical. Fig. 6

453 reveals a slight influence of this species since the addition of pBZQ did not affect
454 considerably the removal rate of DCF.

455 Na_3N has been widely applied for the inhibition of $^1O_2$ contribution (rate constant,
456 $2 \cdot 10^9$ [65]); however, it also reacts with radical species (respective rate constant with
457 $HO^\bullet$ and $SO_4^{\bullet-}$ in the order of 10^{10} [70] and 10^9 M^{-1} s^{-1} [71]). Moreover, the results
458 adding Na_3N must be cautiously analyzed due to the possibility of the reaction of the
459 quencher with PMS molecules, as recently reported by Yang et al [62]. Furthermore, the
460 kinetic reaction of NaN_3 and $O_2^{\bullet-}$ remains still unclear [30]. Since the addition of EtOH
461 or TBA did not inhibit the process, the scavenging effect produced by NaN_3 in this
462 system could only be attributed to the reaction with PMS and/or $^1O_2$. As can be inferred
463 from Fig. 6, no conclusion about a unique contribution of $^1O_2$ can be obtained.
464 However, better results can be extracted when adding furfuryl alcohol (FFA). FFA is
465 also commonly used for the study of $^1O_2$ role (rate constant for the reaction $1.2 \cdot 10^8$ M^{-1}
466 s^{-1} [42,72]). FFA also scavenges $HO^\bullet$ ($1.5 \cdot 10^{10}$ M^{-1} s^{-1} [42]), whose presence have been
467 previously proved to be negligible. The same reasoning can be extrapolated to $SO_4^{\bullet-}$,
468 although no available information about the kinetics with FFA is available. The addition
469 of FFA in the PMS+graphene system led to complete inhibition of the reaction
470 contribution. The DCF degradation obtained was quite similar to that obtained for the
471 adsorption under the same experimental conditions.

472 Summarizing, from the chemical scavenging tests conducted, the main contribution
473 of a non-radical pathway can be envisaged. The presence of π electrons on the surface
474 of graphene enhances the adsorption of the oxidant and organic adsorbates, promoting
475 the oxidation without the presence of free radicals in the media.

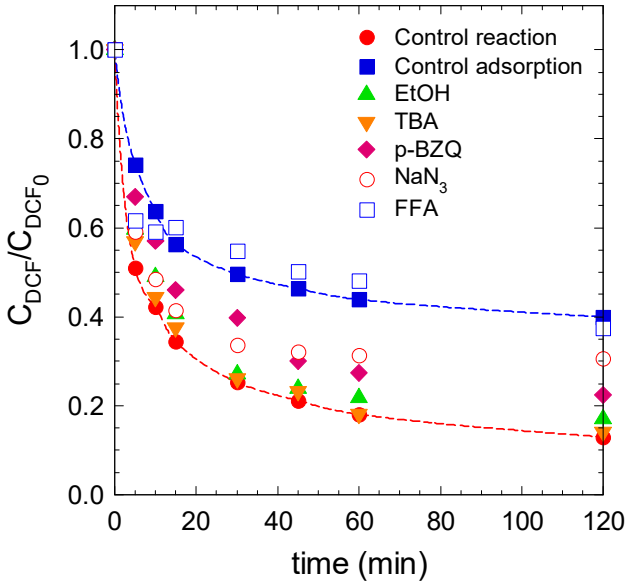

Figure 6. Effect of scavengers on DCF removal during the PMS-catalysis with graphene. Experimental conditions: V=250 mL; $C_{DCF,0}$=5 mg L^{-1}; $C_{PMS,0}$=0.1 mM (except for adsorption control); $C_{graphene}$=20 mg L^{-1}; $pH_{initial}$=4.0-4.4 (before scavenger adding, unbuffered). Concentration of quenchers (when applied), C_{EtOH}=5 mM; C_{TBA}=5 mM; C_{BZQ}=50 μM; C_{NaN3}=10 mM; C_{FFA}=10 mM.

The efficiency of PMS was compared to other common oxidants used for the oxidation of organics, commonly activated by the radical pathway. A series of assays with peroxydisulfate (PDS), hydrogen peroxide (H_2O_2), and peracetic acid (PAA) were carried out (see Fig. 7) for the degradation of DCF by non-radical oxidation on the surface of graphene. Although non-activated direct reaction may take place for certain micropollutants [61,73,74], the direct reaction of DCF with PDS, H_2O_2, and PAA was negligible under the conditions tested. The combination of these oxidants and graphene led to an enhanced DCF depletion if compared to adsorption (54% DCF removal in 2h), the order of reactivity being PMS (87%)~PDS (86%)>PAA (79%)> H_2O_2 (62%). The activation of hydrogen peroxide in graphite [75] and activated carbon [75,76] has been reported to take place, mainly due to the presence of oxygenated surface groups [76]. Recently, PAA activation in carbon fibers has been postulated as more efficient than

H_2O_2 [77], which is a good agreement with the results obtained in this study. The best results of DCF removal were achieved when using PMS or PDS.

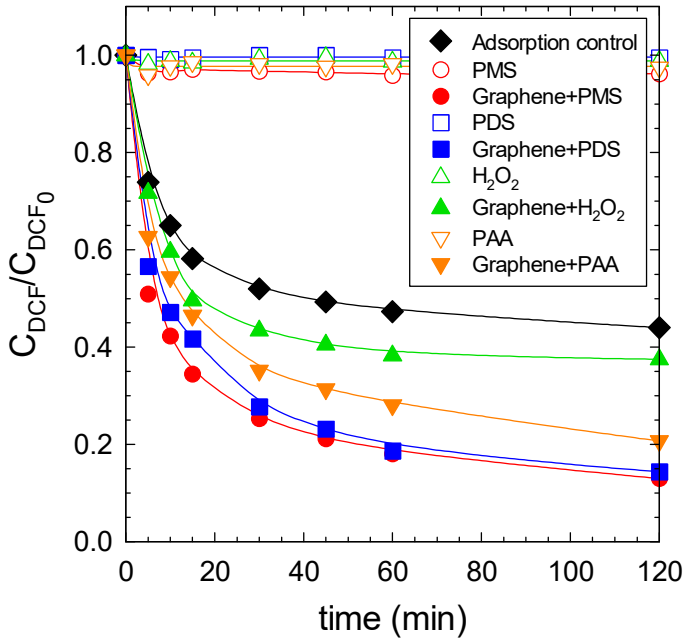

Figure 7. PMS *versus* other oxidants in the catalysis with graphene. Experimental conditions: V=250 mL; $C_{DCF,0}$=5 mg L^{-1}; $C_{oxidant,0}$=0.1 mM (except for adsorption control); $C_{graphene}$=20 mg L^{-1} (when necessary); $pH_{initial}$=4.0-4.4 (unbuffered).

3.3. Peroxymonosulfate-graphene system applied to a mixture of antibiotics

The study applied to diclofenac as target aqueous pollutant was extended to a mixture of three antibiotics, i.e. norfloxacin, tetracycline, and sulfamethoxazole, frequently reported as contaminants of emerging concern [13,78,79]. Thus, Fig. 8 summarizes the results attained for the degradation during the direct oxidation with PMS, the adsorption onto graphene, and the combination of PMS and graphene.

The direct reaction of PMS after 2 h resulted in 20%, 30%, and 85% degradation of norfloxacin, sulfamethoxazole, and tetracycline at initial contaminant: PMS molar ratio of 1:32, 1:25, and 1:44, respectively. Only tetracycline was significantly oxidized by direct reaction with PMS. This behavior has also been reported previously under high

tetracycline: PMS ratio [80]. Sulfamethoxazole and norfloxacin are also expected to undergo direct oxidation with PMS according to the literature [62,81].

The extent of adsorption process depends on the hydrophobic interactions of organic adsorbates and π electrons of graphene as the main route of the adsorption process [9]. The octanol-water partition coefficient (K_{OW}) values can be used as a tool to predict and compare the adsorption affinity of the different target organics. According to the decreasing values of K_{OW}, the adsorption affinity should be sulfamethoxazole > norfloxacin > tetracycline [82]. Nevertheless, the observed order was norfloxacin > tetracycline > sulfamethoxazole. This suggests that not only the hydrophobicity is a determining factor, but also the molecular complexity, the number of aromatic rings, and their spatial distribution play a role, among other factors. All the amount of norfloxacin was completely adsorbed in *ca.* 30 min whereas almost 2 h were necessary for complete adsorption of tetracycline. Only 80% of sulfamethoxazole was absorbed in 2 h, reaching the equilibrium conditions after 90 min.

Considering the different reactivity towards direct oxidation with PMS and the affinity to graphene adsorption for the three antibiotics, the combination of PMS and graphene led to different results. In the case of norfloxacin, due to the high adsorption affinity, no significant improvement in the compound's kinetic removal was achieved when applying PMS and graphene. Tetracycline removal was significantly enhanced when adding PMS, leading to a faster and complete degradation in 15 min. For the case of sulfamethoxazole, the degradation kinetics was also improved.

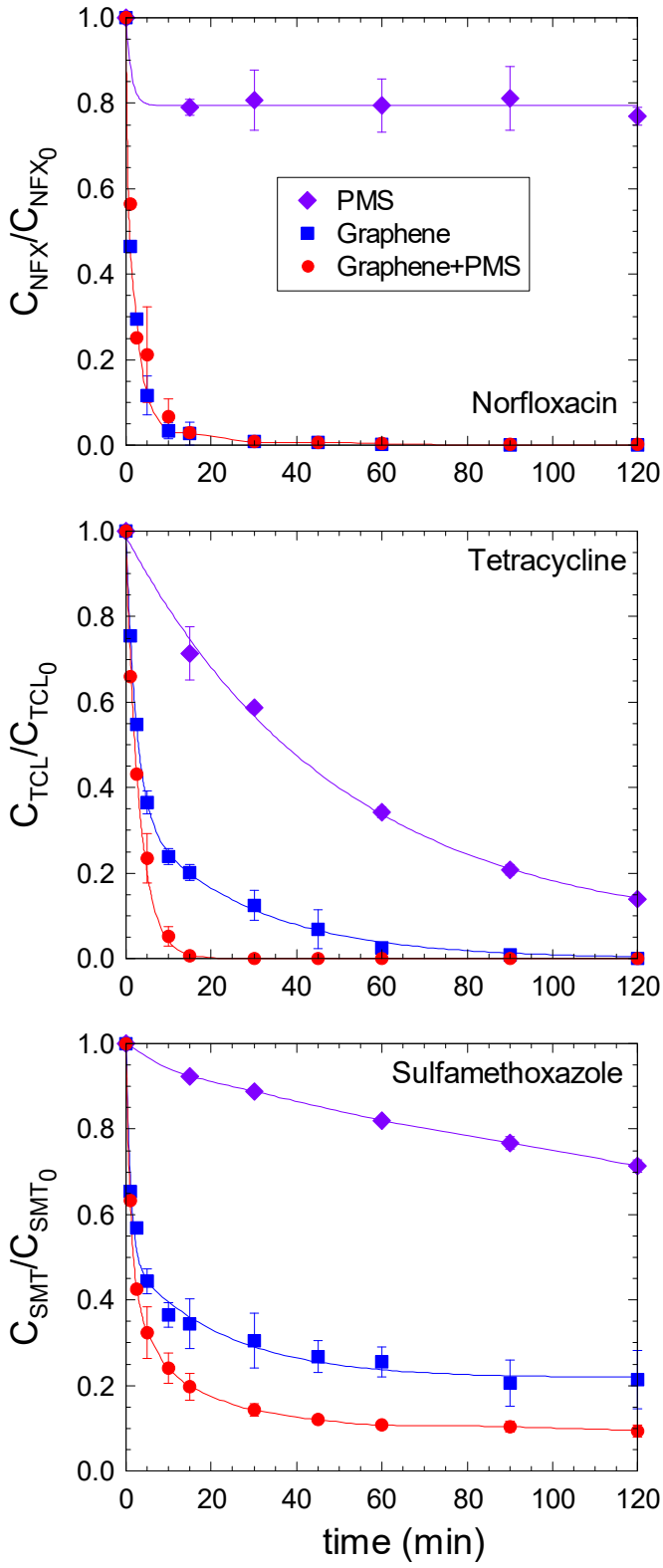

Figure 8. Adsorption *versus* PMS-catalysis onto graphene of a mixture of antibiotics (norfloxacin, tetracycline, and sulfamethoxazole). Experimental conditions: V=250 mL; $C_{i,0}$=5 mg L^{-1} (each); $C_{PMS,0}$=0.5 mM; $C_{graphene}$=100 mg L^{-1}; $pH_{initial}$=4.0-4.8 (unbuffered).

3.4. Graphene characterization before and after oxidative treatment with PMS

The surface properties of the commercial graphene nanoplatelets were studied by means of diverse techniques before and after being in contact with PMS in similar conditions to those developed during the oxidative treatment of pharmaceutical, i.e. ratio C_{PMS}: $C_{graphene}$ = 0.1 mM: 100 mg L^{-1}.

The morphology of the nanoparticles was studied by SEM and TEM microscopy. No differences between the fresh commercial graphene and the PMS treated were observed. From SEM micrographs (Fig. 9), it can be observed that the nanoplatelets are aggregated forming a bigger conglomerate, in some cases over 1µm size. In TEM images (Fig. 9), it is possible to observe the presence of transparent sheets of different shapes and sizes.

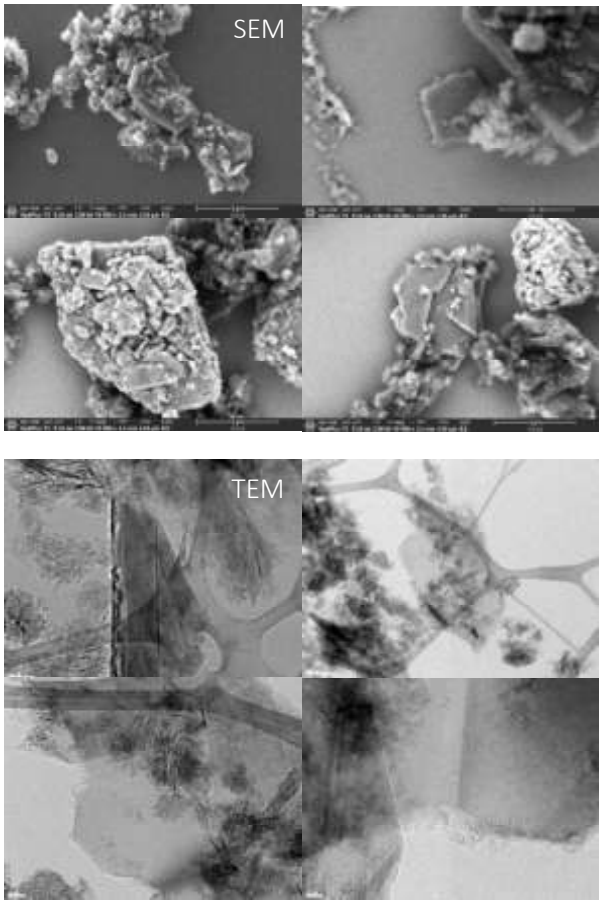

Figure 9. SEM (up) and TEM images (down) of fresh commercial graphene nanoplatelets

550 The specific surface area was determined by N_2 adsorption-desorption isotherm for
551 the fresh commercial graphene and the PMS treated sample. No significant differences
552 before and after the use of PMS were obtained. As shown in Fig. S3, both isotherms
553 describe a reversible II-type isotherm according to IUPAC classification [83]. This
554 behavior of unrestricted multilayer physisorption is characteristic of non-porous
555 materials. Moreover, from the results obtained with the BJH method for pore
556 distribution, a sharp decay in the mesoporous range is observed. Similar results were
557 obtained for the PMS-treated sample (results not shown). The BET specific surface
558 areas obtained were 494±3 and 485±3 m^2 g^{-1} for fresh and PMS-treated graphene,
559 respectively. The initial value is in good agreement with that provided by the
560 manufacturer (500 m^2 g^{-1}). It can be concluded that the material is practically stable and
561 does not lose its N_2 adsorption properties after the addition of PMS for catalytic
562 activation (less than 1.8% of specific surface area loss).
563 Graphene XRD diffractogram is characterized by the presence of broader peaks, low
564 angle displacement, and reduced peaks if compared to the graphite XRD spectrum,
565 which means a larger distance between planes [84]. In the commercial graphene, either
566 before and after using PMS treatment, the main peak appears at *ca.* 26.4º, which is
567 characteristic of the graphitic hexagonal structure [85]. No significant difference in the
568 XRD spectrum after PMS-treatment was registered as shown in Fig. 10. Graphene oxide
569 usually presents a peak around 10º, not observed in this material, attributed to the (001)
570 plane, corresponding to a higher distance between planes if compared to reduced
571 graphene in which this peak disappears leading to the (002) plane [86]. XRD spectrum
572 suggests that the material is stable after being used in PMS catalysis with lack of
573 oxygenated surface groups.

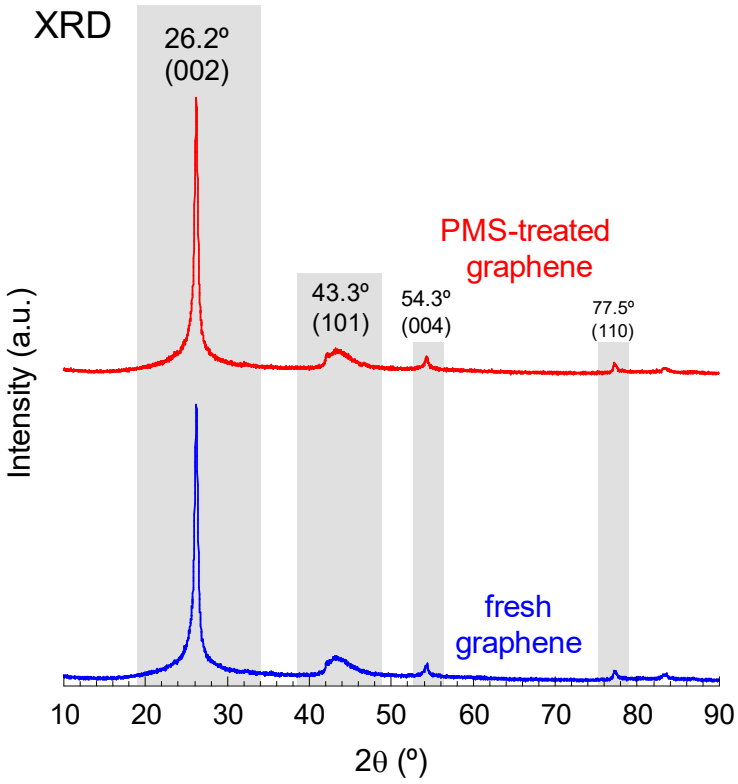

574

575 **Figure 10.** XRD spectra of commercial graphene nanoplatelets before and after PMS-
576 treatment

577 No oxygenated functional groups were observed in FTIR spectra before or after the
578 addition of PMS (see Fig. S4). The lack of significant peaks in FTIR is characteristic of
579 graphitic carbon with a very low proportion of oxygenated groups [85]. Nevertheless,
580 the presence of oxygen in the surface of graphene was further studied by XPS analysis.
581 The high-resolution spectra of O1s region, available in Fig. 11, for the solid before and
582 after the treatment with PMS, presented the contribution of four main oxygenated
583 groups, e.g., carbonyl, hydroxyl, carboxylic and ester [87]. The amount of chemisorbed
584 O_2 was negligible, and the deconvoluted contribution for this chemical state has not
585 been considered in Fig. 11. Table 4 summarizes the contribution percentages of each
586 oxygenated species. As can be observed, after adding PMS, surface hydroxylated and
587 carbonyl groups decreased. Nevertheless, the contribution of C-O and carboxylic groups
588 increased after adding PMS. Recently, a thermodynamics study of the PMS-adsorption

589 into reduced graphene oxide has reported that PMS molecules present tendency to be
590 adsorbed preferably onto C=O as a Lewis basic site [26]. It is thought that the
591 nonbonding electron pair of oxygen in carbonyl group is more attractive to PMS
592 molecule if compared to other oxygenated groups. Moreover, from the atomic total O in
593 each sample, which is very similar, it is deduced that the oxygenation process proceeds
594 through oxidation of hydroxyl to increase the percentage content of carboxylic and
595 ketonic groups.

596 **Table 4.** XPS percentages of oxygenated species of graphene nanoplatelets before and
597 after PMS-treatment

Oxygenated group (%)	Fresh graphene	PMS-treated graphene
C=O	43.8	42.2
C-OH	21.2	16.9
O=C-OH	9.0	14.6
C-O	22.9	26.1
Total atomic O (%)	6.36	6.78

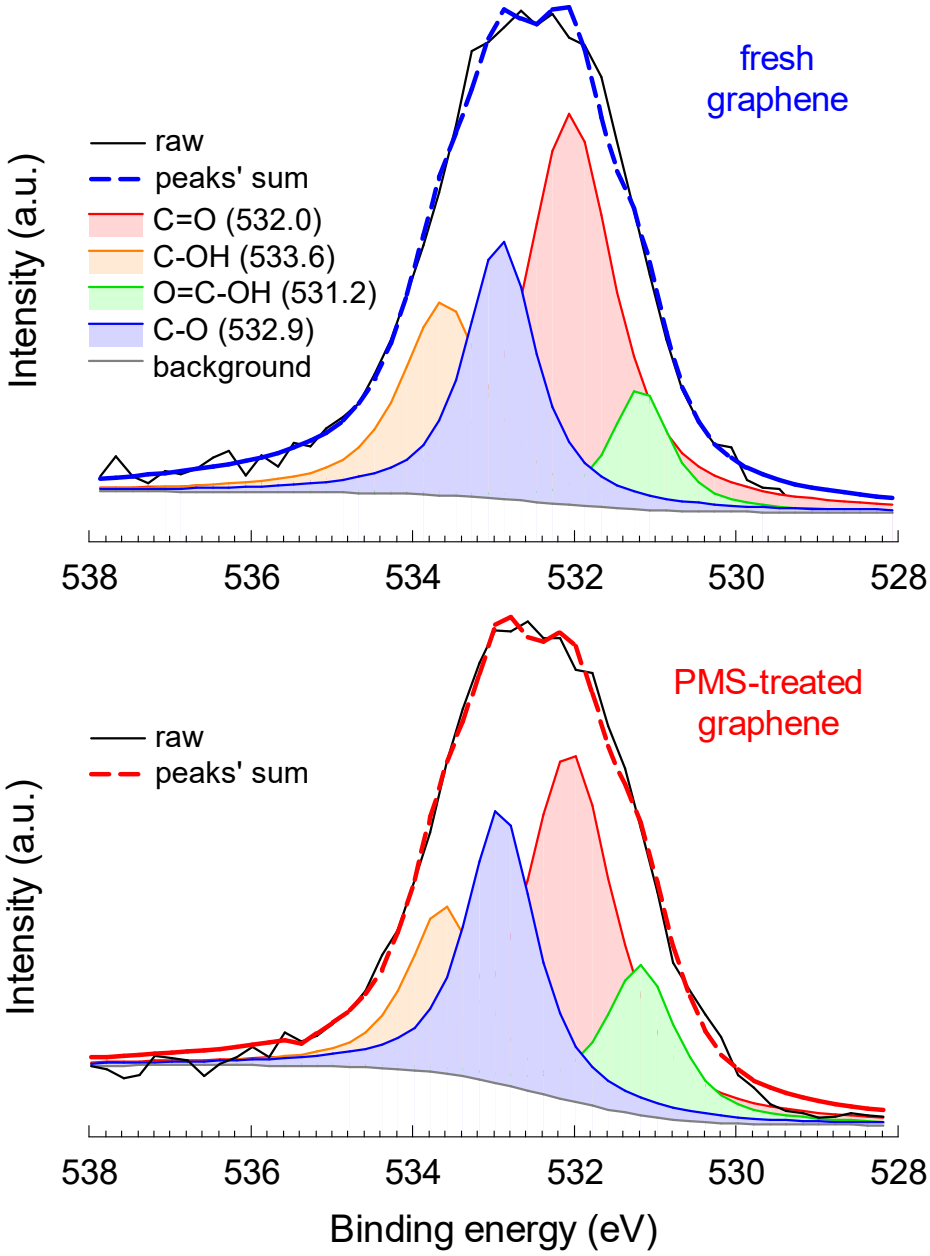

Figure 11. XPS high-resolution spectra of O1s region of commercial graphene nanoplatelets before and after PMS-treatment

4. CONCLUSIONS

The kinetics of the adsorption of PMS onto commercial graphene can be successfully fitted to the Elovich equation. An experimental design showed that initial PMS concentration was the variable that affected the most the rate constant for the process, followed by graphene dose and then slightly by pH.

606 Graphene displayed a high adsorption capacity of the target organic contaminant in
607 water. During diclofenac removal, kinetically speaking, the presence of PMS influenced
608 positively at low doses of graphene, while the effect was less significant at higher doses.
609 This behavior was also observed during the treatment of a mixture of antibiotics
610 (norfloxacin, tetracycline and sulfamethoxazole). Not only the concentration of
611 graphene is crucial in the process, but also the initial pH of the solution that rules the
612 electrical interactions between adsorbates, i.e. diclofenac and oxidant, and graphene.
613 The mechanism of the process was tentatively assessed by quenchers study which
614 revealed the lack of radicals present in the process. The effectiveness of PMS in the
615 catalytic activation of graphene was also compared to peroxydisulfate (PDS), hydrogen
616 peroxide, and peracetic acid (PAA). The reactivity order for diclofenac removal was
617 PMS~PDS>PAA>H_2O_2.
618 Solid characterization of the material revealed high stability towards PMS presence.
619 The adsorption capacity was not compromised as the measured specific surface area
620 after treatment was not altered (1.8% of surface area loss after PMS addition). The
621 morphology and crystallinity did not suffer significant changes. XPS technique showed
622 an increase in the proportion of carboxylic groups coming from the oxidation of surface
623 carbonyl and hydroxylated groups.
624 Further studies on the interaction of the PMS catalytic system with the
625 transformation products and the final oxidation products are encouraged in future work.
626 Also, limitations of this technology such as separation of the solid, its further
627 regeneration, and suitable PMS dosage that does not compromise the release of sulfate
628 need further consideration for real applications.
629

Acknowledgments

Rafael Rodríguez Solís is grateful to *Ramón Areces* Foundation (Madrid, Spain) for his postdoctoral fellowship in the University of Cincinnati (XXX edition of grants for Postgraduate Studies in Life and Matter Sciences in Foreign Universities and Research Centers 2018/2019). Ismael Fernández Mena also acknowledges *MINECO* (Ministry of Economy and Competitiveness) of Spain and *ESF* (European Social Funds) for his predoctoral grant (call 2014, BES-2014-069986). D. D. Dionysiou acknowledges support from the University of Cincinnati through a UNESCO co-Chair Professor position on "Water Access and Sustainability" and the Herman Schneider Professorship in the College of Engineering and Applied Sciences.

Authors would like to express their gratitude to the *Advanced Materials Characterization Center* of the University of Cincinnati (Ohio, USA) and *Materials Characterization Facility* of the University of Notre Dame (Indiana, USA) for the help with the analysis of graphene samples.

References

[1] K.S. Novoselov, A.K. Geim, S. V Morozov, D. Jiang, Y. Zhang, S. V Dubonos, I. V Grigorieva, A.A. Firsov, Electric field effect in atomically thin carbon films, Science. 306 (2004) 666–669. doi:10.1126/science.1102896.

[2] S. Stankovich, D.A. Dikin, G.H.B. Dommett, K.M. Kohlhaas, E.J. Zimney, E.A. Stach, R.D. Piner, S.T. Nguyen, R.S. Ruoff, Graphene-based composite materials, Nature. 442 (2006) 282–286. doi:10.1038/nature04969.

[3] Y. Han, Z. Xu, C. Gao, Ultrathin Graphene Nanofiltration Membrane for Water Purification, Adv. Funct. Mater. 23 (2013) 3693–3700. doi:10.1002/adfm.201202601.

[4] M. Hu, B. Mi, Enabling Graphene Oxide Nanosheets as Water Separation Membranes, Environ. Sci. Technol. 47 (2013) 3715–3723. doi:10.1021/es400571g.

[5] D. Cohen-Tanugi, J.C. Grossman, Water Desalination across Nanoporous Graphene, Nano Lett. 12 (2012) 3602–3608. doi:10.1021/nl3012853.

[6] J.R. Werber, C.O. Osuji, M. Elimelech, Materials for next-generation desalination and water purification membranes, Nat. Rev. Mater. 1 (2016) 16018. doi:10.1038/natrevmats.2016.18.

[7] S. Chowdhury, R. Balasubramanian, Recent advances in the use of graphene-family nanoadsorbents for removal of toxic pollutants from wastewater, Adv. Colloid Interface Sci. 204 (2014) 35–56. doi:10.1016/J.CIS.2013.12.005.

[8] J. Xu, L. Wang, Y. Zhu, Decontamination of Bisphenol A from Aqueous Solution by Graphene Adsorption, Langmuir. 28 (2012) 8418–8425. doi:10.1021/la301476p.

[9] G. Ersan, O.G. Apul, F. Perreault, T. Karanfil, Adsorption of organic contaminants by graphene nanosheets: A review, Water Res. 126 (2017) 385–398. doi:10.1016/J.WATRES.2017.08.010.

[10] R.K. Upadhyay, N. Soin, S.S. Roy, Role of graphene/metal oxide composites as photocatalysts, adsorbents and disinfectants in water treatment: a review, RSC Adv. 4 (2014) 3823–3851. doi:10.1039/C3RA45013A.

[11] Z. Cai, A.D. Dwivedi, W.-N. Lee, X. Zhao, W. Liu, M. Sillanpää, D. Zhao, C.-H. Huang, J. Fu, Application of nanotechnologies for removing pharmaceutically active compounds from water: development and future trends, Environ. Sci.

677 Nano. 5 (2018) 27–47. doi:10.1039/C7EN00644F.

678 [12] L. Meng, Y. Sun, H. Gong, P. Wang, W. Qiao, L. Gan, L. Xu, Research progress
679 of the application of graphene-based materials in the treatment of water
680 pollutants, Carbon N. Y. (2019). doi:10.1016/J.CARBON.2019.06.092.

681 [13] I. Michael, L. Rizzo, C.S. McArdell, C.M. Manaia, C. Merlin, T. Schwartz, C.
682 Dagot, D. Fatta-Kassinos, Urban wastewater treatment plants as hotspots for the
683 release of antibiotics in the environment: A review, Water Res. 47 (2013) 957–
684 995. doi:10.1016/J.WATRES.2012.11.027.

685 [14] M. Gavrilescu, K. Demnerová, J. Aamand, S. Agathos, F. Fava, Emerging
686 pollutants in the environment: present and future challenges in biomonitoring,
687 ecological risks and bioremediation, N. Biotechnol. 32 (2015) 147–156.
688 doi:10.1016/J.NBT.2014.01.001.

689 [15] B. Petrie, R. Barden, B. Kasprzyk-Hordern, A review on emerging contaminants
690 in wastewaters and the environment: Current knowledge, understudied areas and
691 recommendations for future monitoring, Water Res. 72 (2015) 3–27.
692 doi:10.1016/J.WATRES.2014.08.053.

693 [16] I. Oller, S. Malato, J.A. Sánchez-Pérez, Combination of Advanced Oxidation
694 Processes and biological treatments for wastewater decontamination—A review,
695 Sci. Total Environ. 409 (2011) 4141–4166.
696 doi:10.1016/J.SCITOTENV.2010.08.061.

697 [17] S. Guerra-Rodríguez, E. Rodríguez, D.N. Singh, J. Rodríguez-Chueca, S. Guerra-
698 Rodríguez, E. Rodríguez, D.N. Singh, J. Rodríguez-Chueca, Assessment of
699 Sulfate Radical-Based Advanced Oxidation Processes for Water and Wastewater
700 Treatment: A Review, Water. 10 (2018) 1828. doi:10.3390/w10121828.

[18] D.B. Miklos, C. Remy, M. Jekel, K.G. Linden, J.E. Drewes, U. Hübner, Evaluation of advanced oxidation processes for water and wastewater treatment – A critical review, Water Res. 139 (2018) 118–131. doi:10.1016/J.WATRES.2018.03.042.

[19] S.K. Alharbi, W.E. Price, Degradation and Fate of Pharmaceutically Active Contaminants by Advanced Oxidation Processes, Curr. Pollut. Reports. 3 (2017) 268–280. doi:10.1007/s40726-017-0072-6.

[20] C. Liang, H.-W. Su, Identification of Sulfate and Hydroxyl Radicals in Thermally Activated Persulfate, Ind. Eng. Chem. Res. 48 (2009) 5558–5562. doi:10.1021/ie9002848.

[21] S. Wacławek, H. V. Lutze, K. Grübel, V.V.T. Padil, M. Černík, D.D. Dionysiou, Chemistry of persulfates in water and wastewater treatment: A review, Chem. Eng. J. 330 (2017) 44–62. doi:10.1016/J.CEJ.2017.07.132.

[22] F. Ghanbari, M. Moradi, Application of peroxymonosulfate and its activation methods for degradation of environmental organic pollutants: Review, Chem. Eng. J. 310 (2017) 41–62. doi:10.1016/J.CEJ.2016.10.064.

[23] L.W. Matzek, K.E. Carter, Activated persulfate for organic chemical degradation: A review, Chemosphere. 151 (2016) 178–188. doi:10.1016/J.CHEMOSPHERE.2016.02.055.

[24] X. Duan, Z. Ao, L. Zhou, H. Sun, G. Wang, S. Wang, Occurrence of radical and nonradical pathways from carbocatalysts for aqueous and nonaqueous catalytic oxidation, Appl. Catal. B Environ. 188 (2016) 98–105. doi:10.1016/J.APCATB.2016.01.059.

[25] Q. Zhao, Q. Mao, Y. Zhou, J. Wei, X. Liu, J. Yang, L. Luo, J. Zhang, H. Chen, H. Chen, L. Tang, Metal-free carbon materials-catalyzed sulfate radical-based advanced oxidation processes: A review on heterogeneous catalysts and applications, Chemosphere. 189 (2017) 224–238. doi:10.1016/J.CHEMOSPHERE.2017.09.042.

[26] X. Duan, H. Sun, Z. Ao, L. Zhou, G. Wang, S. Wang, Unveiling the active sites of graphene-catalyzed peroxymonosulfate activation, Carbon N. Y. 107 (2016) 371–378. doi:10.1016/j.carbon.2016.06.016.

[27] J. Wang, X. Duan, Q. Dong, F. Meng, X. Tan, S. Liu, S. Wang, Facile synthesis of N-doped 3D graphene aerogel and its excellent performance in catalytic degradation of antibiotic contaminants in water, Carbon N. Y. 144 (2019) 781–790. doi:10.1016/J.CARBON.2019.01.003.

[28] X. Duan, Z. Ao, D. Li, H. Sun, L. Zhou, A. Suvorova, M. Saunders, G. Wang, S. Wang, Surface-tailored nanodiamonds as excellent metal-free catalysts for organic oxidation, Carbon N. Y. 103 (2016) 404–411. doi:10.1016/J.CARBON.2016.03.034.

[29] C. Wang, J. Kang, H. Sun, H.M. Ang, M.O. Tadé, S. Wang, One-pot synthesis of N-doped graphene for metal-free advanced oxidation processes, Carbon N. Y. 102 (2016) 279–287. doi:10.1016/J.CARBON.2016.02.048.

[30] X. Duan, H. Sun, Z. Shao, S. Wang, Nonradical reactions in environmental remediation processes: Uncertainty and challenges, Appl. Catal. B Environ. 224 (2018) 973–982. doi:10.1016/J.APCATB.2017.11.051.

[31] Y. Wang, M. Liu, X. Zhao, D. Cao, T. Guo, B. Yang, Insights into heterogeneous catalysis of peroxymonosulfate activation by boron-doped ordered mesoporous

748 carbon, Carbon N. Y. 135 (2018) 238–247.
749 doi:10.1016/J.CARBON.2018.01.106.

750 [32] Y. Zhou, J. Jiang, Y. Gao, J. Ma, S.-Y. Pang, J. Li, X.-T. Lu, L.-P. Yuan,
751 Activation of Peroxymonosulfate by Benzoquinone: A Novel Nonradical
752 Oxidation Process, Environ. Sci. Technol. 49 (2015) 12941–12950.
753 doi:10.1021/acs.est.5b03595.

754 [33] X. Cheng, H. Guo, Y. Zhang, X. Wu, Y. Liu, Non-photochemical production of
755 singlet oxygen via activation of persulfate by carbon nanotubes, Water Res. 113
756 (2017) 80–88. doi:10.1016/J.WATRES.2017.02.016.

757 [34] X. Duan, Z. Ao, H. Zhang, M. Saunders, H. Sun, Z. Shao, S. Wang,
758 Nanodiamonds in sp2/sp3 configuration for radical to nonradical oxidation: Core-
759 shell layer dependence, Appl. Catal. B Environ. 222 (2018) 176–181.
760 doi:10.1016/J.APCATB.2017.10.007.

761 [35] H. Sun, S. Liu, G. Zhou, H.M. Ang, M.O. Tadé, S. Wang, Reduced Graphene
762 Oxide for Catalytic Oxidation of Aqueous Organic Pollutants, ACS Appl. Mater.
763 Interfaces. 4 (2012) 5466–5471. doi:10.1021/am301372d.

764 [36] W. Peng, S. Liu, H. Sun, Y. Yao, L. Zhi, S. Wang, Synthesis of porous reduced
765 graphene oxide as metal-free carbon for adsorption and catalytic oxidation of
766 organics in water, J. Mater. Chem. A. 1 (2013) 5854–5859.
767 doi:10.1039/c3ta10592j.

768 [37] S. Indrawirawan, H. Sun, X. Duan, S. Wang, Nanocarbons in different structural
769 dimensions (0–3D) for phenol adsorption and metal-free catalytic oxidation,
770 Appl. Catal. B Environ. 179 (2015) 352–362.
771 doi:10.1016/J.APCATB.2015.05.049.

772 [38] T. Olmez-Hanci, I. Arslan-Alaton, S. Gurmen, I. Gafarli, S. Khoei, S. Safaltin, D.
773 Yesiltepe Ozcelik, Oxidative degradation of Bisphenol A by carbocatalytic
774 activation of persulfate and peroxymonosulfate with reduced graphene oxide, J.
775 Hazard. Mater. 360 (2018) 141–149. doi:10.1016/J.JHAZMAT.2018.07.098.

776 [39] J.N. Miller, J.C. Miller, R.D. Miller, Statistics and chemometrics for analytical
777 chemistry, Seventh ed, Pearson Education Limited, Harlow (United Kingdom),
778 2018.

779 [40] S. Gokulakrishnan, A. Mohammed, H. Prakash, Determination of persulphates
780 using N,N-diethyl-p-phenylenediamine as colorimetric reagent: Oxidative
781 coloration and degradation of the reagent without bactericidal effect in water,
782 Chem. Eng. J. 286 (2016) 223–231. doi:10.1016/J.CEJ.2015.10.058.

783 [41] Z. Rajah, M. Guiza, R.R. Solís, N. Becheikh, F.J. Rivas, A. Ouederni, Clopyralid
784 degradation using solar-photocatalytic/ozone process with olive stone activated
785 carbon, J. Environ. Chem. Eng. 7 (2019) 102900.
786 doi:10.1016/J.JECE.2019.102900.

787 [42] X. Chen, W.-D. Oh, T.-T. Lim, Graphene- and CNTs-based carbocatalysts in
788 persulfates activation: Material design and catalytic mechanisms, Chem. Eng. J.
789 354 (2018) 941–976. doi:10.1016/J.CEJ.2018.08.049.

790 [43] C. Aharoni, F.C. Tompkins, Kinetics of Adsorption and Desorption and the
791 Elovich Equation, Adv. Catal. 21 (1970) 1–49. doi:10.1016/S0360-
792 0564(08)60563-5.

793 [44] K. Thakur, B. Kandasubramanian, Graphene and Graphene Oxide-Based
794 Composites for Removal of Organic Pollutants: A Review, J. Chem. Eng. Data.
795 64 (2019) 833–867. doi:10.1021/acs.jced.8b01057.

796 [45] S.H. Chien, W.R. Clayton, Application of Elovich Equation to the Kinetics of
797 Phosphate Release and Sorption in Soils, Soil Sci. Soc. Am. J. 44 (1980) 265–
798 268. doi:10.2136/sssaj1980.03615995004400020013x.

799 [46] B.N. Bhadra, P.W. Seo, S.H. Jhung, Adsorption of diclofenac sodium from water
800 using oxidized activated carbon, Chem. Eng. J. 301 (2016) 27–34.
801 doi:10.1016/J.CEJ.2016.04.143.

802 [47] J.L. Sotelo, A. Rodríguez, S. Álvarez, J. García, Removal of caffeine and
803 diclofenac on activated carbon in fixed bed column, Chem. Eng. Res. Des. 90
804 (2012) 967–974. doi:10.1016/J.CHERD.2011.10.012.

805 [48] E.-E. Chang, J.-C. Wan, H. Kim, C.-H. Liang, Y.-D. Dai, P.-C. Chiang,
806 Adsorption of Selected Pharmaceutical Compounds onto Activated Carbon in
807 Dilute Aqueous Solutions Exemplified by Acetaminophen, Diclofenac, and
808 Sulfamethoxazole., Sci. World J. 2015 (2015) 186501. doi:10.1155/2015/186501.

809 [49] S. Larous, A.-H. Meniai, Adsorption of Diclofenac from aqueous solution using
810 activated carbon prepared from olive stones, Int. J. Hydrogen Energy. 41 (2016)
811 10380–10390. doi:10.1016/J.IJHYDENE.2016.01.096.

812 [50] R. Baccar, M. Sarrà, J. Bouzid, M. Feki, P. Blánquez, Removal of
813 pharmaceutical compounds by activated carbon prepared from agricultural by-
814 product, Chem. Eng. J. 211–212 (2012) 310–317.
815 doi:10.1016/J.CEJ.2012.09.099.

816 [51] C. Saucier, M.A. Adebayo, E.C. Lima, R. Cataluña, P.S. Thue, L.D.T. Prola, M.J.
817 Puchana-Rosero, F.M. Machado, F.A. Pavan, G.L. Dotto, Microwave-assisted
818 activated carbon from cocoa shell as adsorbent for removal of sodium diclofenac
819 and nimesulide from aqueous effluents, J. Hazard. Mater. 289 (2015) 18–27.

820 doi:10.1016/J.JHAZMAT.2015.02.026.

821 [52] J.L. Sotelo, A.R. Rodríguez, M.M. Mateos, S.D. Hernández, S.A. Torrellas, J.G.
822 Rodríguez, Adsorption of pharmaceutical compounds and an endocrine disruptor
823 from aqueous solutions by carbon materials, J. Environ. Sci. Heal. Part B. 47
824 (2012) 640–652. doi:10.1080/03601234.2012.668462.

825 [53] H. Zhao, X. Liu, Z. Cao, Y. Zhan, X. Shi, Y. Yang, J. Zhou, J. Xu, Adsorption
826 behavior and mechanism of chloramphenicols, sulfonamides, and non-antibiotic
827 pharmaceuticals on multi-walled carbon nanotubes, J. Hazard. Mater. 310 (2016)
828 235–245. doi:10.1016/J.JHAZMAT.2016.02.045.

829 [54] A. Gil, L. Santamaría, S.A. Korili, Removal of Caffeine and Diclofenac from
830 Aqueous Solution by Adsorption on Multiwalled Carbon Nanotubes, Colloid
831 Interface Sci. Commun. 22 (2018) 25–28. doi:10.1016/J.COLCOM.2017.11.007.

832 [55] S.-W. Nam, C. Jung, H. Li, M. Yu, J.R.V. Flora, L.K. Boateng, N. Her, K.-D.
833 Zoh, Y. Yoon, Adsorption characteristics of diclofenac and sulfamethoxazole to
834 graphene oxide in aqueous solution, Chemosphere. 136 (2015) 20–26.
835 doi:10.1016/J.CHEMOSPHERE.2015.03.061.

836 [56] I.M. Jauris, C.F. Matos, C. Saucier, E.C. Lima, A.J.G. Zarbin, S.B. Fagan, F.M.
837 Machado, I. Zanella, Adsorption of sodium diclofenac on graphene: a combined
838 experimental and theoretical study, Phys. Chem. Chem. Phys. 18 (2016) 1526–
839 1536. doi:10.1039/C5CP05940B.

840 [57] B.Y.Z. Hiew, L.Y. Lee, K.C. Lai, S. Gan, S. Thangalazhy-Gopakumar, G.-T.
841 Pan, T.C.-K. Yang, Adsorptive decontamination of diclofenac by three-
842 dimensional graphene-based adsorbent: Response surface methodology,
843 adsorption equilibrium, kinetic and thermodynamic studies, Environ. Res. 168

(2019) 241–253. doi:10.1016/J.ENVRES.2018.09.030.

[58] K.Y. Foo, B.H. Hameed, Insights into the modeling of adsorption isotherm systems, Chem. Eng. J. 156 (2010) 2–10. doi:10.1016/J.CEJ.2009.09.013.

[59] S.-W. Nam, C. Jung, H. Li, M. Yu, J.R.V. Flora, L.K. Boateng, N. Her, K.-D. Zoh, Y. Yoon, Adsorption characteristics of diclofenac and sulfamethoxazole to graphene oxide in aqueous solution, Chemosphere. 136 (2015) 20–26. doi:10.1016/J.CHEMOSPHERE.2015.03.061.

[60] Y. Ji, J. Lu, L. Wang, M. Jiang, Y. Yang, P. Yang, L. Zhou, C. Ferronato, J.-M. Chovelon, Non-activated peroxymonosulfate oxidation of sulfonamide antibiotics in water: Kinetics, mechanisms, and implications for water treatment, Water Res. 147 (2018) 82–90. doi:10.1016/j.watres.2018.09.037.

[61] J. Chen, C. Fang, W. Xia, T. Huang, C.-H. Huang, Selective Transformation of β-Lactam Antibiotics by Peroxymonosulfate: Reaction Kinetics and Nonradical Mechanism, Environ. Sci. Technol. 52 (2018) 1461–1470. doi:10.1021/acs.est.7b05543.

[62] Y. Yang, G. Banerjee, G.W. Brudvig, J.-H. Kim, J.J. Pignatello, Oxidation of Organic Compounds in Water by Unactivated Peroxymonosulfate, Environ. Sci. Technol. 52 (2018) 5911–5919. doi:10.1021/acs.est.8b00735.

[63] R.R. Solís, F.J. Rivas, M. Tierno, Monopersulfate photocatalysis under 365 nm radiation. Direct oxidation and monopersulfate promoted photocatalysis of the herbicide tembotrione, J. Environ. Manage. 181 (2016) 385–394. doi:10.1016/j.jenvman.2016.06.061.

[64] R.J. Kennedy, A.M. Stock, The Oxidation of Organic Substances by Potassium

867 Peroxymonosulfate, J. Org. Chem. 25 (1960) 1901–1906.
868 doi:10.1021/jo01081a019.

869 [65] F. Ghanbari, M. Moradi, Application of peroxymonosulfate and its activation
870 methods for degradation of environmental organic pollutants: Review, Chem.
871 Eng. J. 310 (2017) 41–62. doi:https://doi.org/10.1016/j.cej.2016.10.064.

872 [66] P. Shukla, I. Fatimah, S. Wang, H.M. Ang, M.O. Tadé, Photocatalytic generation
873 of sulphate and hydroxyl radicals using zinc oxide under low-power UV to
874 oxidise phenolic contaminants in wastewater, Catal. Today. 157 (2010) 410–414.
875 doi:10.1016/j.cattod.2010.04.015.

876 [67] M. Hayyan, M.A. Hashim, I.M. AlNashef, Superoxide Ion: Generation and
877 Chemical Implications, Chem. Rev. 116 (2016) 3029–3085.
878 doi:10.1021/acs.chemrev.5b00407.

879 [68] M. Nien Schuchmann, E. Bothe, J. von Sonntag, C. von Sonntag, Reaction of OH
880 radicals with benzoquinone in aqueous solutions. A pulse radiolysis study, J.
881 Chem. Soc. Perkin Trans. 2. (1998) 791–796. doi:10.1039/A708772A.

882 [69] P. Neta, R.E. Huie, A.B. Ross, Rate Constants for Reactions of Peroxyl Radicals
883 in Aqueous Solution, Aqueous Solut. J. Phys. Chem. Ref. Data. 17 (1988) 1027–
884 1284. doi:10.1063/1.555808.

885 [70] I. Kraljić, C.N. Trumbore, p-Nitrosodimethylaniline as an OH Radical Scavenger
886 in Radiation Chemistry, J. Am. Chem. Soc. 87 (1965) 2547–2550.
887 doi:10.1021/ja01090a004.

888 [71] P. Neta, R.E. Huie, A.B. Ross, Rate Constants for Reactions of Inorganic
889 Radicals in Aqueous Solution, J. Phys. Chem. Ref. Data. 17 (1988) 1027–1284.

890 doi:10.1063/1.555808.

891 [72] W.R. Haag, J. Hoigné, E. Gassman, A.M. Braun, Singlet oxygen in surface
892 waters — Part I: Furfuryl alcohol as a trapping agent, Chemosphere. 13 (1984)
893 631–640. doi:10.1016/0045-6535(84)90199-1.

894 [73] K. Zhang, X. Zhou, P. Du, T. Zhang, M. Cai, P. Sun, C.-H. Huang, Oxidation of
895 β-lactam antibiotics by peracetic acid: Reaction kinetics, product and pathway
896 evaluation, Water Res. 123 (2017) 153–161.
897 doi:10.1016/J.WATRES.2017.06.057.

898 [74] Y. Zhou, Y. Gao, S.-Y. Pang, J. Jiang, Y. Yang, J. Ma, Y. Yang, J. Duan, Q.
899 Guo, Oxidation of fluoroquinolone antibiotics by peroxymonosulfate without
900 activation: Kinetics, products, and antibacterial deactivation, Water Res. 145
901 (2018) 210–219. doi:10.1016/J.WATRES.2018.08.026.

902 [75] F. Lücking, H. Köser, M. Jank, A. Ritter, Iron powder, graphite and activated
903 carbon as catalysts for the oxidation of 4-chlorophenol with hydrogen peroxide in
904 aqueous solution, Water Res. 32 (1998) 2607–2614. doi:10.1016/S0043-
905 1354(98)00016-5.

906 [76] A. Rey, J.A. Zazo, J.A. Casas, A. Bahamonde, J.J. Rodriguez, Influence of the
907 structural and surface characteristics of activated carbon on the catalytic
908 decomposition of hydrogen peroxide, Appl. Catal. A Gen. 402 (2011) 146–155.
909 doi:10.1016/J.APCATA.2011.05.040.

910 [77] F. Zhou, C. Lu, Y. Yao, L. Sun, F. Gong, D. Li, K. Pei, W. Lu, W. Chen,
911 Activated carbon fibers as an effective metal-free catalyst for peracetic acid
912 activation: Implications for the removal of organic pollutants, Chem. Eng. J. 281
913 (2015) 953–960. doi:10.1016/J.CEJ.2015.07.034.

914 [78] M.J. Focazio, D.W. Kolpin, K.K. Barnes, E.T. Furlong, M.T. Meyer, S.D. Zaugg,
915 L.B. Barber, M.E. Thurman, A national reconnaissance for pharmaceuticals and
916 other organic wastewater contaminants in the United States — II) Untreated
917 drinking water sources, Sci. Total Environ. 402 (2008) 201–216.
918 doi:10.1016/J.SCITOTENV.2008.02.021.

919 [79] O.M. Rodriguez-Narvaez, J.M. Peralta-Hernandez, A. Goonetilleke, E.R.
920 Bandala, Treatment technologies for emerging contaminants in water: A review,
921 Chem. Eng. J. 323 (2017) 361–380. doi:10.1016/J.CEJ.2017.04.106.

922 [80] Q. Yang, X. Yang, Y. Yan, C. Sun, H. Wu, J. He, D. Wang, Heterogeneous
923 activation of peroxymonosulfate by different ferromanganese oxides for
924 tetracycline degradation: Structure dependence and catalytic mechanism, Chem.
925 Eng. J. 348 (2018) 263–270. doi:10.1016/J.CEJ.2018.04.206.

926 [81] L. Chen, D. Ding, C. Liu, H. Cai, Y. Qu, S. Yang, Y. Gao, T. Cai, Degradation of
927 norfloxacin by $CoFe_2O_4$-GO composite coupled with peroxymonosulfate: A
928 comparative study and mechanistic consideration, Chem. Eng. J. 334 (2018)
929 273–284. doi:10.1016/J.CEJ.2017.10.040.

930 [82] O. Ursu, J. Holmes, J. Knockel, C.G. Bologa, J.J. Yang, S.L. Mathias, S.J.
931 Nelson, T.I. Oprea, DrugCentral: online drug compendium, Nucleic Acids Res.
932 45 (2017) D932–D939. doi:10.1093/nar/gkw993.

933 [83] M. Thommes, K. Kaneko, A. V Neimark, J.P. Olivier, F. Rodriguez-Reinoso, J.
934 Rouquerol, K.S.W. Sing, Physisorption of gases, with special reference to the
935 evaluation of surface area and pore size distribution (IUPAC Technical Report),
936 Pure Appl. Chem. 87 (2015) 1–19. doi:10.1515/pac-2014-1117.

937 [84] C. Monteserín, M. Blanco, E. Aranzabe, A. Aranzabe, J.M. Laza, A. Larrañaga-

938 Varga, J.L. Vilas, C. Monteserín, M. Blanco, E. Aranzabe, A. Aranzabe, J.M.
939 Laza, A. Larrañaga-Varga, J.L. Vilas, Effects of Graphene Oxide and
940 Chemically-Reduced Graphene Oxide on the Dynamic Mechanical Properties of
941 Epoxy Amine Composites, Pol. 9 (2017) 449. doi:10.3390/polym9090449.

942 [85] M.A. Saiful Badri, M.M. Salleh, N.F. Md Noor, M.Y.A. Rahman, A.A. Umar,
943 Green synthesis of few-layered graphene from aqueous processed graphite
944 exfoliation for graphene thin film preparation, Mater. Chem. Phys. 193 (2017)
945 212–219. doi:10.1016/j.matchemphys.2017.02.029.

946 [86] A. Jabbar, G. Yasin, W.Q. Khan, M. Yousaf Anwar, R.M. Korai, M.N. Nizam,
947 G. Muhyodin, Electrochemical deposition of nickel graphene composite coatings:
948 effect of deposition temperature on its surface morphology and corrosion
949 resistance, RSC Adv. 7 (2017) 31100–31109. doi:10.1039/c6ra28755g.

950 [87] Y.J. Oh, J.J. Yoo, Y. Il Kim, J.K. Yoon, H.N. Yoon, J.-H. Kim, S. Bin Park,
951 Oxygen functional groups and electrochemical capacitive behavior of
952 incompletely reduced graphene oxides as a thin-film electrode of supercapacitor,
953 Electrochim. Acta. 116 (2014) 118–128.
954 doi:10.1016/J.ELECTACTA.2013.11.040.